Engineering and Technology Journal
Journal homepage: https://etj.uotechnology.edu.iq

Effect of tool profile on micro hardness, forming limit, and final thickness in incremental hole flanging process of DC01 steel and AA1050 sheet metals

Hunar M. Tahir M. Ali *, **Hameed D. Lafta, Ayad F. Shahab**

Mechanical and Manufacturing Engineering Department, Technical College of Engineering, Sulaimani Polytechnic University, Sulaimani, Kurdistan Region, Iraq.
*Corresponding authors Email: hunar.mmuhammad.t@spu.edu.iq ; hameed.lafta@spu.edu.iq; ayad.shahab@spu.edu.iq

HIGHLIGHTS

- Maximum hardness was 73% and 15% for DC01 0.7, 1mm at72° and 90°, respectively.
- Highest hardness was 6%, 8% for AA1050 at forming angle of 90° for 0.7 and 1 mm.
- Maximum thickness reduction of 40%, 51%for1mmDC01 and AA1050 thicknesses.
- Variation flange-thickness can be controlled by careful selection of process parameters in hole flanging.

ARTICLE INFO

Handling editor: Omar H. Hassoon

Keywords:
Incremental forming
Hole-flanging
Forming limit
Tool profile
Micro hardness

ABSTRACT

The present study delves into the incremental hole flanging process applied to AA1050 and DC01 sheet metals with 0.7 and 1 mm thicknesses. Employing a distinctive lathe-based fixture, the process utilizes a proposed tool profile and fixture incorporating mutually spinning and rolling motions. The investigation covers three forming angles (72°, 90°, and 45°) and three different rotational forming speeds (170, 350, and 525 RPM). The primary objective is to assess the impact of tool forming angle, forming speeds on microhardness, thickness ratio, and forming limit diagram. The study employs a microhardness test, measurements of flange height, and final thickness. Results revealed hardness and thickness variations depending on material type sheet thickness, showing a critical forming speed at which a critical change in variation trend occurs irrespective of forming angle. Forming speed and tool profile were selected carefully to produce a maximum forming limit and a large amount of plastic deformation with no failure of metals. Hardness distribution experienced smooth variation, and the maximum increase in post hardness didn't exceed 73% without evidence of crack formation at the end of the process. As well as the thickness distribution shows a uniform variation along the flange profile with a maximum thickness reduction of 40% and 51% for 1 mm DC01 and AA1050 sheets, respectively. Finally, based on the proposed tool geometry and holding arrangement adopted in the present work, results indicated a good enhancement in forming limit is satisfied with no obvious large thinning occurring due to change in deformation modes can be used successfully in incremental hole flanging process.

1. Introduction

Hole-flanging represents a frequently used shaping process, particularly within the automotive and aeronautical industries. This procedure entails securing a sheet of material with a pre-existing hole and reshaping the material around the hole using a single punch motion. The primary objectives of hole-flanging are to enhance the durability of the hole's perimeter, enhance its aesthetic quality, and offer supplementary reinforcement for connecting sheet components [1]. Hole flanging is a critical step in sheet metal manufacturing, involving the creation of flanges in pre-cut hole sheets. This process strengthens the flanges and allows for precise connections and positioning of components. Recent research suggests that using a progressive shaping method instead of traditional hole-flanging methods could be more cost-effective and eliminate the need for expensive equipment. Traditional methods can be costly due to tooling expenses, making affordable metal forming equipment crucial for small-batch production, and combining hole flanging with an incremental sheet forming process (ISFP) is a smart choice in such scenarios. However, the incremental sheet-forming process is considered an economically viable procedure, and it can be entirely executed on numerically controlled machines or machines specially designed for ISF applications [2]. A fixture is

http://doi.org/10.30684/etj.2024.146281.1677
Received 22 January 2024; Received in revised form 21 February 2024; Accepted 08 March 2024; Available online 14 April 2024
2412-0758/University of Technology-Iraq, Baghdad, Iraq

needed to secure the sheet, and a punch is used to deform the sheet layer-by-layer to shape the required form, as depicted in Figure 1.

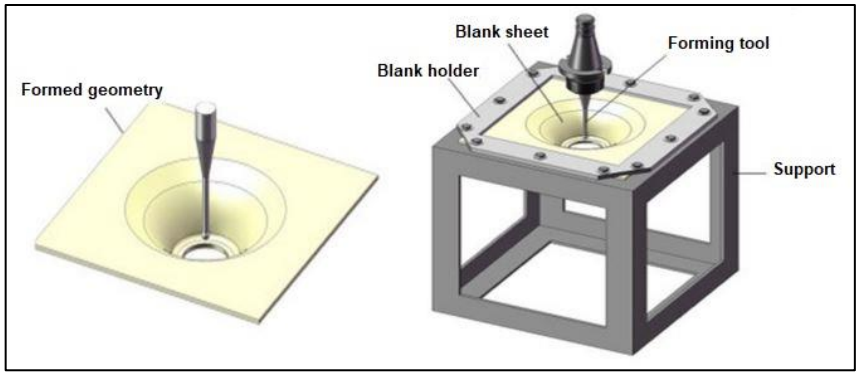

Figure 1: Incremental hole flanging setup [2]

The incremental sheet forming (ISF) processes are significantly affected by forming parameters, including forming angle, incremental depth, forming speed, tool size and shape, and tool path, on formability, deformation, failure mechanics, accuracy, and surface roughness. The importance of comprehending how these parameters impact different materials and forming conditions to optimize the ISF process [3].

However, in the incremental hole flanging process reducing the contact surface radius can enhance a material's forming limit, yet it adversely affects the surface quality of the resulting part. Employing an end tool, or a combination of end tools, is the preferred approach for achieving the best outcomes in Single Point Incremental Forming (SPIF). This implies that judiciously choosing and utilizing the right end tool(s) can improve the forming limit and the surface quality of the formed parts [4].

Kumar et al. [5] studied the effect of the punch profile on the deformation behavior of the AA5052 sheet in the stretch flanging process. They focused on the influence of various punch profiles on the formation of the stretch flange. Finite elements simulation and experimental validation are employed to compare the results concerning edge crack, forming load, and strain distribution. It is indicated by the findings that the deformation behavior is significantly influenced by the punch profile, with the hemispherical punch profile exhibiting the most favorable results. Differences in dimple size and distribution for various punch profiles are also revealed through fractography analysis. Durante et al. [6] investigated experimentally the influence of tool rotational speed on forming forces in an incremental forming process of AA7075-T0 sheets by using a steel punch with a hemispherical head. The results indicated that the forming forces are affected by tool rotation, showing a decrease in force peaks when the tool is rotating. Additionally, the study provides insights into the effects of tool rotation on the incremental forming process. Besong et al. [7] improved hole-flanging formability by focusing on punch rotation relying on temperature and strain rate-dependent forming limit curves. It is demonstrated through simulations and experiments that formability is enhanced in hole-flanging when employing punch rotation compared to conventional methods. The effects of temperature, strain rate, and process parameters on formability are also investigated. Results suggest that heightened formability is achieved with high-speed punch rotation and elevated temperatures, which substantially increases the maximum hole expansion ratio. Laugwitz et al. [8] studied high-speed hole-flanging using Single Point Incremental Forming (SPIF) on a lathe machine to speed up processing. To further improve the precision of the flange geometry, they also used a tool design that employed four pivot-mounted forming tools with an 18mm diameter. The design's simplicity allows a great deal of flexibility. It easily compares incremental hole flanging processes carried out using conventional 3-axis CNC machines by utilizing the incremental sheet forming (ISF) technique. All instruments have also undergone heat treatment, improving their capacity to withstand deterioration over time. Silva et al. [9] discussed the formability of hole-flanging using incremental sheet forming as an alternative to conventional press-working. The influence of material failure, specifically by necking and fracture, on the limiting forming ratio is investigated in this study. The effectiveness of this technique was explored using Aluminum A-H111 blanks of 1mm thickness and Titanium (grade 2) blanks of 0.7 mm thickness. The focus of the investigation is to evaluate the incremental sheet-forming process in creating flanges on pre-cut hole blanks made of these materials, thorough analysis of the resulting components, the success of the hole-flanging process, and determine the optimal parameters for achieving desirable outcomes. Gandla et al. [10] examined different wall angles, including 45°, 60°, 75°, and 90°, to produce the dome shape. They utilized the Master Cam software to create a spiral tool path, facilitating the formation of the various shapes. The experiments maintained fixed process parameters with a constant spindle speed of 250 rpm. Their study is based on a proposed theoretical analysis and numerical simulation to predict the thickness variation throughout the forming process. The results showed that the thickness distribution, forming forces, and geometrical accuracy agree with the experimental results. Montanari et al. [11] proved that using the circle grid analysis technique is crucial in investigating the strains involved in hole flanging utilizing Single Point Incremental Forming (SPIF). This approach enables formability prediction through forming limit diagrams (FLD) by accurately identifying the failure points within the primary strain space. This involves the application of a grid of circles ranging from 2 to 2.5 mm in diameter onto the sheet surface through methods such as screen printing or electrochemical etching prior to deformation. A specific area of interest is designated to conduct a thorough strain analysis, which will serve as the strain path after deformation. The results indicated that the griding technique offered a

comprehensive analysis of the strain progression. Cristino et al. [12] proposed an analysis for tracking the deformation history in hole-flanging by the SPIF technique, combining the circle-grid approach with a versatile version specifically tailored for aluminum AA1050 to account for anisotropic plastic flow. This approach is based on the principle that plastic deformation during hole-flanging follows proportional strain paths, with the slope β representing the ratio of in-plane strains ε_2 and ε_1. The in-plane strain measurement makes this method precise and reliable. In this engaging conversation about deformation mechanics in hole-flanging using SPIF, it is brought to attention that while the flange walls experience almost entirely plane strain conditions, the hole edges undergo equal amounts of bi-axial stretching. An interesting observation is that there are no changes in strain or stress paths as the material goes from necking to fracture, suggesting that the failure in this process is directly caused by excessive thinning rather than localized necking. This raises important questions about the limitations of SPIF in this scenario and prompts further exploration. Laugwitz et al.[13] Introduced a novel, portable single-point strain analysis system for sheet metal forming applications. This advanced system utilizes a USB microscope with various end caps to capture images. Developed with Python and the Open CV library, it features a user-friendly GUI for effortless user interaction. The improved and inexpensive USB microscope camera modifications minimize interference from reflective surfaces on metal sheets. This efficient system adheres to the ASTM E2218-02 standard for accurate strain measurements and can also print a 1 mm grid to measure strains. Rigorous validation tests show a mean absolute deviation of strain measurements at approximately - 0.009, ensuring reliable results. Mezher et al. [14] examined the Forming Limit Diagram (FLD) in relation to the single point incremental forming (SPIF) method for sheet metals AA1050 and DC04, with the X and Y axes representing the genuine minor and major strains, respectively. The forming angle affected both the DC04 and AA1050 sheet metals FLD curves. Greater wall angles were linked to significant major and minor stresses, indicating that formability decreased as the forming angle rose. Two unique zones were seen in the FLD curves: some points indicated biaxial strain circumstances, while others indicated uniaxial strain levels. The findings strongly agreed with the experimental data, indicating a trustworthy correlation between the two techniques and offering insightful information on how the materials behave under varying forming circumstances.

In a recent study, Mezher et al. [15] utilized AA1050 aluminum alloy and DC04 carbon steel sheets, both 1 mm thick, were used in the experiment. As part of the single point incremental forming (SPIF) procedure, the sheets were bent into a variety of wall angles, including 45°, 55°, 65°, 70°, and 75°, to ascertain the safe formability limit of each sheet metal. After finishing each experiment, the researchers checked the finished product for signs of fractures. The objective was to determine the largest forming angle that could be reached without fracturing the material. This data is essential for streamlining the SPIF procedure and guaranteeing the flawless production of sheet metal components. The forming limit diagram (FLD) shows the extremely effected of the rising of the forming angle, and the critical major and minor strains were generated with higher wall angles. DC04 carbon steel at different wall angles exhibits roughly good results compared to AA1050 aluminum alloy. Vasile et al. [16] Focused on analyzing the forming capacity of steel blanks with the hydroforming process. Steel sheets have been in focus for numerical and experimental analysis for this research. The main advantages of these materials are good surface finish, excellent forming capacity, and close tolerances, which are appealing advantages for manufacturers. A finite element model has been developed from data obtained through tensile tests and forming limit curves. A newly developed hydroforming press has been used for forming experiments. Side-by-side analysis between numerical and experimental results concludes the experiment. Centeno et al. and Montanari et al. [11,17] Conducted a study on the effects of pre-cut holes on the stresses that resulted from the multi-stage incremental sheet-forming process of 1 mm thick AA1050-H111 blanks. The main objective was to investigate how adding pre-cut holes affected the materials capacity to endure deformation throughout the forming process. The researchers learned more about the material's behavior and how it reacted to the forming process by analyzing the stresses that resulted. Their research offers useful data for streamlining the production of sheet metal components. The combination of plasticity with data from circle-grid analysis allows setting up an experimentally based approach for tracing the history of material strains. It stresses against the formability limits in the principal strain and stress spaces. This result differs from that commonly found in hole-flanging produced by conventional press working, which fails by necking under tension-compression strain loading paths [9]. Mezher and Shakir [18] employed an experimental investigation and numerical validation to analyze the impact of SPIHF process parameters like tool diameter, feed rate, spindle speed, and initial hole diameter on the post-forming hardness property, the forming limit diagram (FLD), and spring-back aspects for the truncated incrementally formed components made from AA1060 aluminum alloy and DC01 carbon steel. The plasticity behavior of both sheet metals was simulated using the Workbench LS-DYNA model and ANSYS software version 18. Additionally, Cowper Symonds power-law hardening was added to the model to account for material properties. The results indicated that greater spindle speed and bigger pre-cut holes were shown to significantly increase the post-formed hardness of the truncated components. In contrast, the converse was seen when using a higher feed rate and a larger tool diameter. In addition, the FLD and spring-back improved dramatically with larger hole diameters. Puche [19] studied the critical analysis of the hole flanging operation by Single Point Incremental Forming (SPIF), which is performed in one stage, from the point of view of material formability and the geometrical capabilities of the process. To understand and quantify the advantages of a single-stage SPIF operation, an experimental campaign of hole flanging tests by both incremental and conventional forming was performed on an aluminum alloy 7075-O sheet. A detailed study of the evolution of the strains in the flange is provided. The mechanisms and modes of failure of the sheet and characterization of the flange ability in both operations were analyzed using a forming limit diagram (FLD). The effect of bending induced by the tool in SPIF and the punch edge radius in conventional forming was clearly elucidated with the flange geometry and the forming forces. The comparison performed in this study enables the identification of the technological advantages and limitations in the hole-flanging process by single-stage SPIF.

The objective of the present study is to overcome a notable challenge observed in the traditional sheet-forming process, characterized by a substantial reduction in sheet thickness leading to an uneven distribution of thickness in the final products. To address this issue, a proposed technique combining more than one deformation mode (spinning and rolling) with a tool profile provided by a wide range of forming angles (45^o to 90^o) may be adopted to form the flange in the hole flanging process based on incremental forming technology. The effect of forming angle and forming speed, using different types of materials, on hardness and thickness distributions are analyzed experimentally. Further, the effect of material type and thickness on the forming limit diagram and flange height are presented and discussed.

2. Experimental work

2.1 Material selection

The selection of the materials adopted in the present work is based on the extensive utilization of these materials in various industrial fields, such as the automotive and aerospace industries. Two types of sheet metals are used to prepare the specimens in the present experimental work. These materials are aluminum alloy sheets AA1050 and mild low carbon steel sheet DC01 with two different thicknesses of 0.7 mm and 1 mm for both metal sheets. The aim behind using two different types of materials and thicknesses is because the hole flanging process effectiveness is influenced by various factors, including tool design, sheet metal properties, thickness, rotational speed, and wall angles. Therefore, delving into the flanging process using these different thicknesses can offer a comprehensive understanding of its intricacies. The mechanical properties of the materials are evaluated by tensile test using the United universal testing machine SHFM-600kN, as shown in Table 1 below.

Table 1: Mechanical properties of AA1050 aluminum alloy and DC01 carbon steel

Material	Type	Thickness (mm)	Yield Strength (MPa)	Ultimate tensile Strength (MPa)
DC01	Mild low-carbon steel	0.7	356	416.91
DC01	Mild low-carbon steel	1	427	485.07
AA1050	Aluminum alloy	0.7	25	156.42
AA1050	Aluminum alloy	1	50	180

2.2 Specimens preparation and gridding

The specimens shape, and dimensions are designed to meet the requirements of the proposed incremental hole-flanging tools adopted in the present work. The specimens are firstly designed using AUTOCAD software in a circular shape of 150 mm diameter with a central hole of 20 mm. Also, the specimens are provided with an additional equally spaced 6 holes of 10 mm diameter at a diametric circle of 140 mm to be used to fix the specimen in the specimen holder firmly. Finally, the designed specimens are produced using expertly high-precision CNC laser cutting machine. Experimental Work Layout is shown (a) Sample Preparation (b) Hole Flanging Experimental Procedure (c) Grid Data Collection, Sample Preparation for Tests Hardness and Surface Quality (d) Laboratory Tests Hardness and Surface Quality in Figure 2 and a detailed flow chart in Figure 3.

For gridding, the specimens are equipped with a net of circles of 3 mm diameter over a 100 mm diametric circle. To streamline the gridding process, a fiber laser marking machine was implemented to generate a (3 mm) circle on the surface of each specimen within a (100 mm) range. The gridding process presents a refined and practical experimental methodology carried out to measure the strains and changes in thickness along the profiles of the hole-flanged specimens [13]. The workpiece Preparation a) Cut specimen, and b) Final gridded specimen are shown in Figure 4 b.

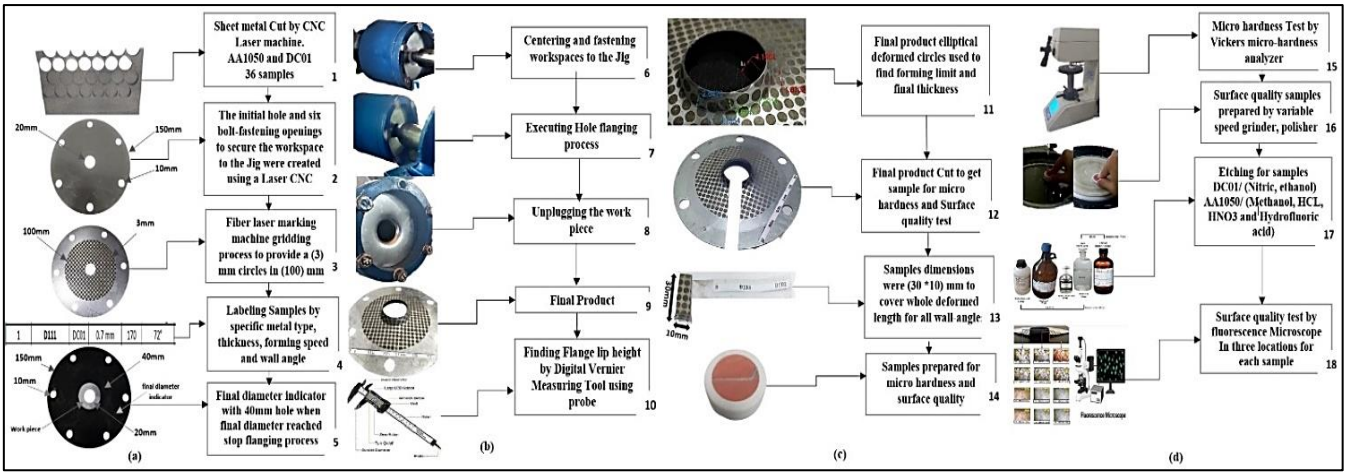

Figure 2: Experimental Work Layout (a) Sample Preparation (b) Hole Flanging Experimental Procedure (c) Grid Data Collection, Sample Preparation for Tests: Hardness and Surface Quality (d) Laboratory Tests: Hardness and Surface Quality

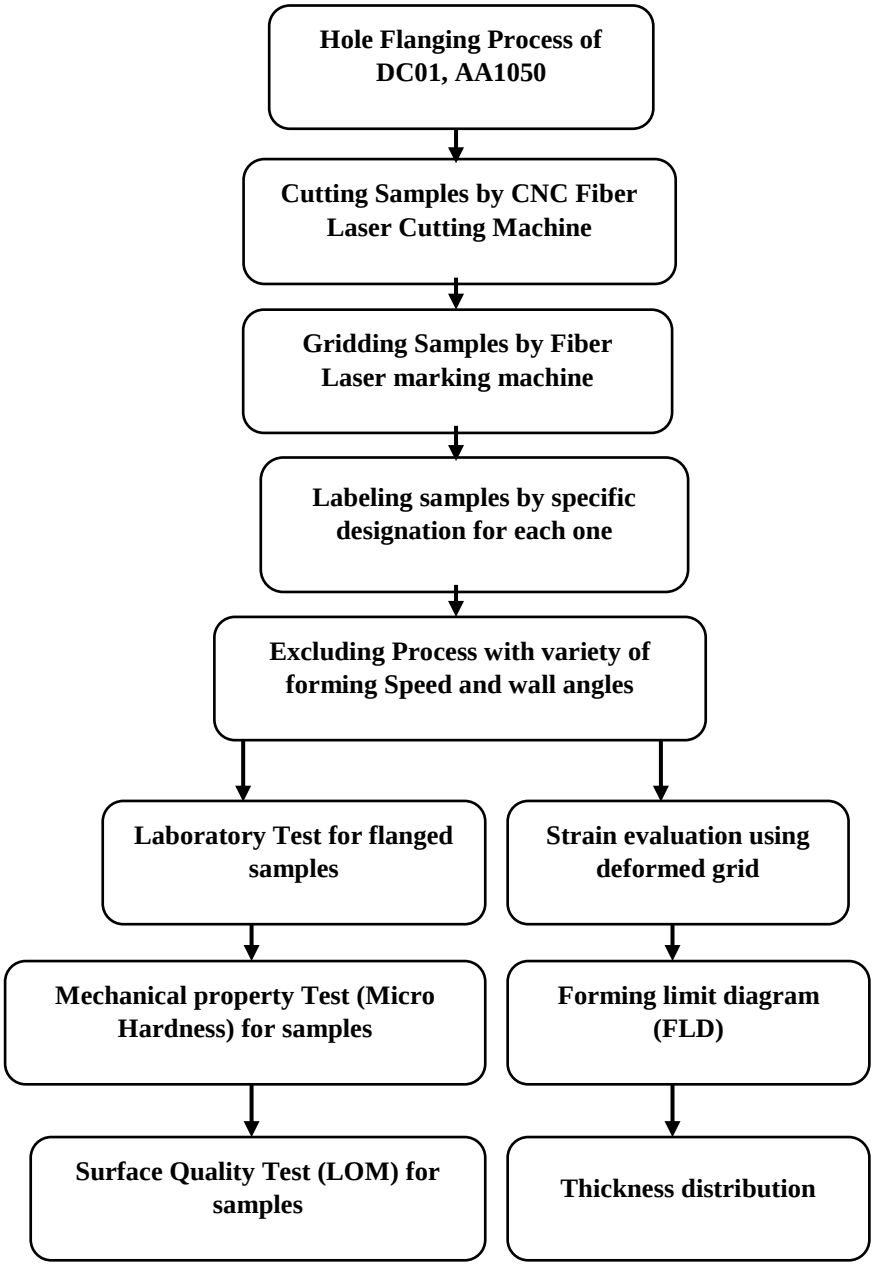

Figure 3: Experimental Flow Chart

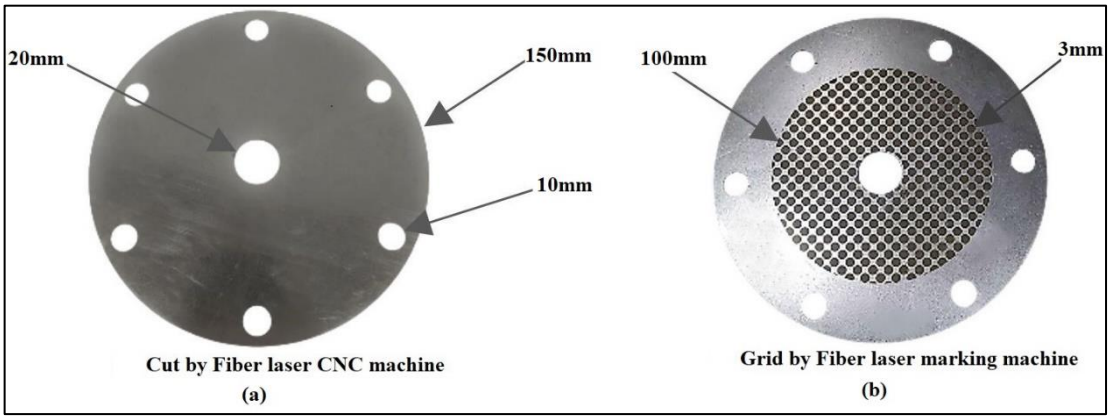

Figure 4: Workpiece Preparation a) Cut specimen, and b) Final gridded specimen

2.3 Hole flanging tooling

The single-pass hole flanging process uses a 2-axis lath machine equipped with the developed hole flanging tools. The experimental setup is shown in Figure 5. The single incremental hole flanging set up comprised of three parts. The specimen holder (Jig), the hole flanging tool, and the tool fixture.

The specimen fixture consists of a 30 mm thick hollow circular backing plate (Jig) of 150 mm diameter and 200 mm length, with one end equipped with shank of 100 mm diameter and 100 mm height to be clamped by the lathe chuck. The second end carrying out the specimen holder, which consists of a ring, has six holes, each of 10 mm diameter, and is securely attached to the specimen fixture using six M17 bolts to firmly fix the gridded specimen, as shown in Figure 6.

The tool and tool holder are shown in Figure 7. The tool has a con profile with a 40 mm diameter extended over a 60 mm length and provided an end shank of 110 mm length and 25 mm diameter to be fitted with three ball bearings to permit a free rotational motion of the tool about the longitudinal tool axis. The tool is fixed to the tool holder that is designed to be incorporated into the tool post of the lathe machine through an appropriate tool fixture that consists of a circular cylinder with an internal hole fitted with the size of the ball bearing and welded to two parallel bars of 2*2 cm^2 of square section and 160 mm apart to be firmly sited on the tool post. The tool hardened through torch quenching and rapid cooling in water to room temperature and ground to impart a high-quality surface finish.

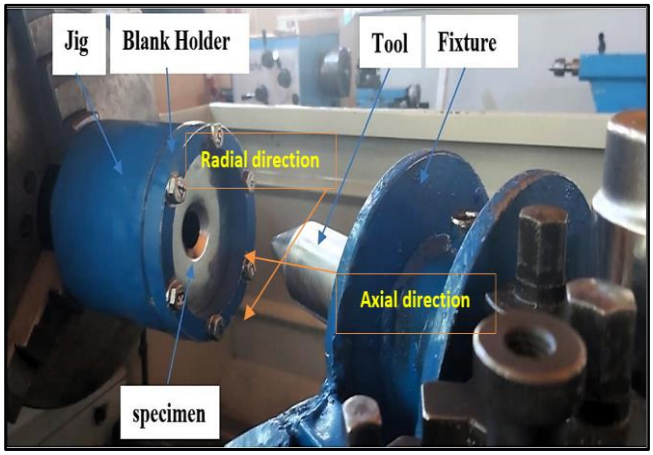

Figure 5: Experimental setup for incremental hole flanging process

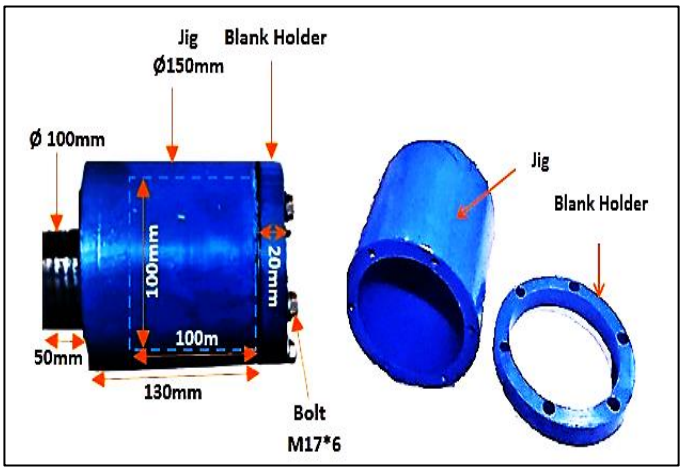

Figure 6: Holflanging Workpiece Setup Jig

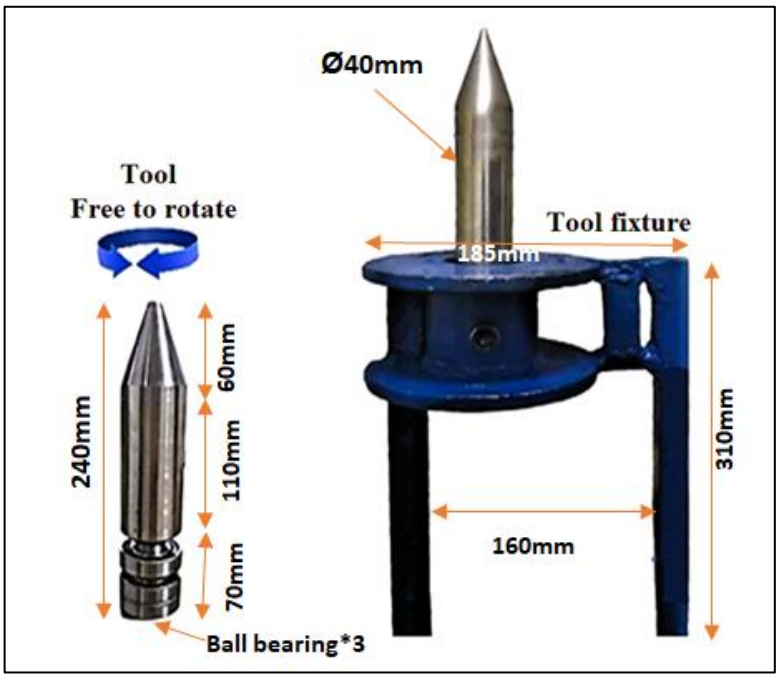

Figure 7: Hole Flanging Tool and Tool fixture

2.4 Hole flanging process

The hole flanging process is carried out by firmly setting the specimen holder into the lath chuck, then firming the gridded specimen into the specimen holder. The next step starts by correctly and accurately adjusting the wall angle between the specimen face and the tapered face of the tool to provide three angle walls of 45°, 72°, and 90°, which are used later in incremental hole flanging experimental work over a range of forming speed (specimen rotation speed), as shown in Figure 8 below. Formability significantly increased with higher spindle speed and sheet thickness. A successful forming of components without fracture was achieved with higher spindle speed and sheet thickness. The correlation between increased formability and sheet thickness is linked to the material's mechanical properties. The significance of adjusting the forming angle (wall angle) impacts the flange profile formed by the hole flanging process. To study the effect of forming speed, material type, and thickness on different characteristics of the incremental hole flanging process using the prosed tool profile, the experiments were conducted by keeping all parameters constant except the one under test, as shown in Figure 9.

The circular grid analysis was used in the present work to measure the strains through different zones of the formed specimen. The primary strain ε1 is analyzed using the true strain's definition as appear in equation 1 and 2 [20]:

$$\varepsilon_1 = \int_{L_o}^{L_1} \frac{dL}{L} = ln(\frac{L_1}{L_o}) \quad (1)$$

$$\varepsilon_2 = \int_{L_o}^{L_2} \frac{dL}{L} = ln(\frac{L_2}{L_o}) \quad (2)$$

Where, Lo represents the original diameter of the gridded circles before deformation, L_1 denotes the large diameter of the deformed gridded circle (ellipse) after deformation, and L_2 represents the small diameter of the deformed gridded circle (ellipse).

The AUTOCAD program is used to assess the measurements of the deformed gridded circles at three specific points for each specimen: the beginning of the deformation, the middle of the lip (corner), and the end of the lip, as illustrated in Figure 9. This analysis aimed to identify both the minor and major strains. An accuracy of 0.000 mm indicates a very high level of precision in dimension measurement for an elliptical shape. The variation in specimen thickness along the flange profile by calculating the thickness strain using the volume constancy in equation 3, such that [25].

$$\varepsilon_1 + \varepsilon_2 + \varepsilon_t = 0 \quad (3)$$

Finally, the thickness can be determined by equation 4:

$$t_{final} = t_o \times e^{\varepsilon_t} \quad (4)$$

where the t_{final} and t_o are the initial and final specimen thickness at each location.

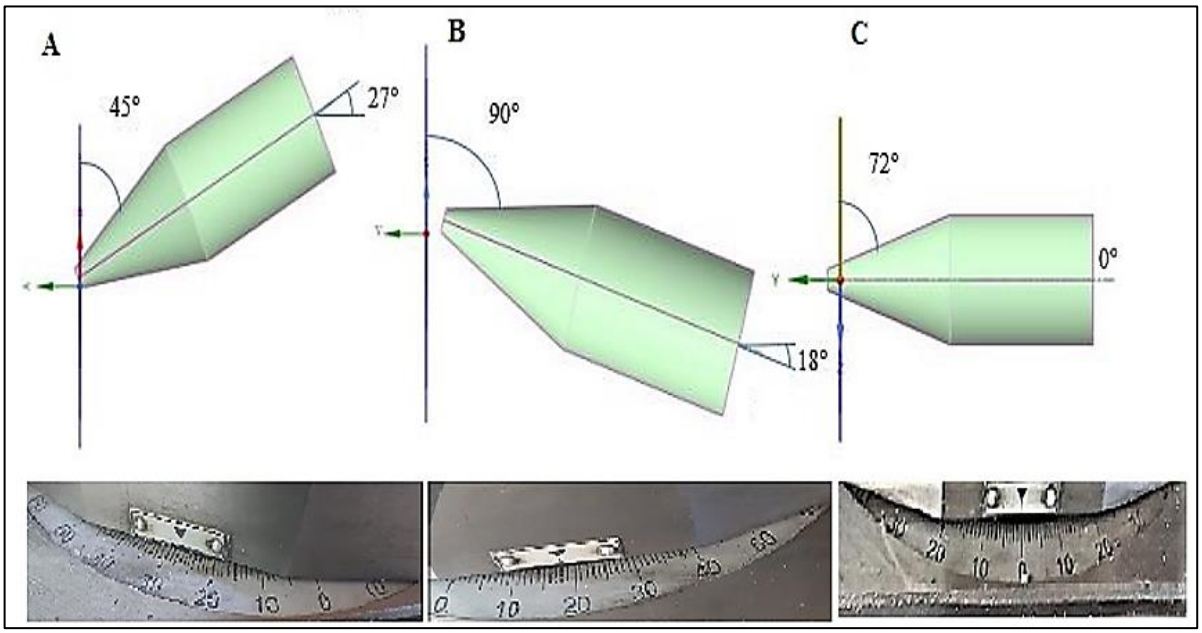

Figure 8: Tool Angle 18° and Tool Post Angles,Wall Angles Relations A) Tool post angle of 27° to achieve a wall angle of 45° B) Tool post angle of 18° to achieve a wall angle of 90° C) Tool post angle of 0° to achieve a wall angle of 72°

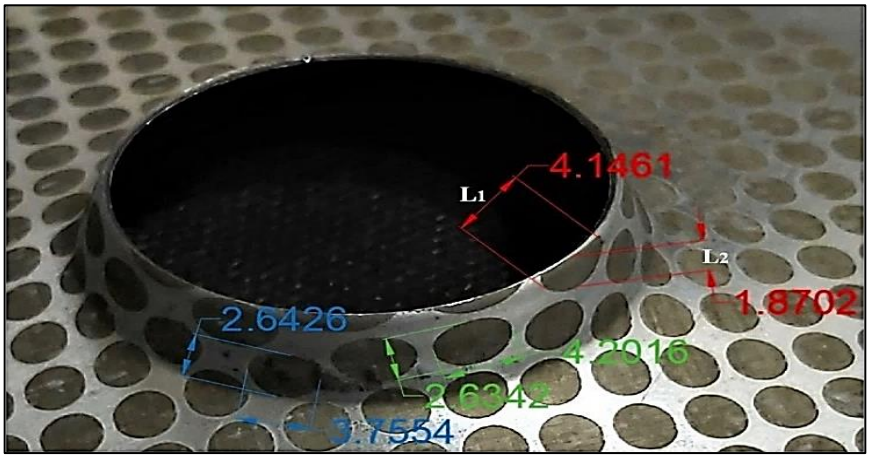

Figure 9: Strain Measurement of Deformed Grids, L1: Measurement for Major Strain, L2: Measurement for Minor Strain, Blue: Initial Forming Stage, Green: Middle Stage of Forming, Red: End Stage of Forming, Utilizing AutoCAD for Analysis

2.5 Microhardness test

A Vickers micro-hardness analyzer was used to evaluate the specimens' micro-hardness before the hole flanging process for comparison purposes and after the hole flanging process for determining the hardness distribution along the flange profile, as shown in Figure 10.

The samples' hardness was measured at ambient temperature using Vickers hardness tester (T-Test) per the ASTM E92-17 standard hardness test [21]. The micro-hardness examination was carried out by pushing a square-based pyramidal diamond indenter with 136° face angles for some time according to the material type. The hardness measurement is repeated several times at least three points at the same location for accurate measurement. All specimens are sectioned, cleaned, polished, and mounted in epoxy mounts prior to testing, as shown in Figure 11. The hardness test starts by imposing a 5 kg load for 15 seconds during the measurement process for low-carbon steel specimens, while a 1 kg load is imposed for 15 seconds during the hardness measurement for AA1050 specimens, as shown in Figure 12. The hardness tester provided the hardness measurement with an accuracy of (± 0.0001) HV, as appeared by the digital screen of the device.

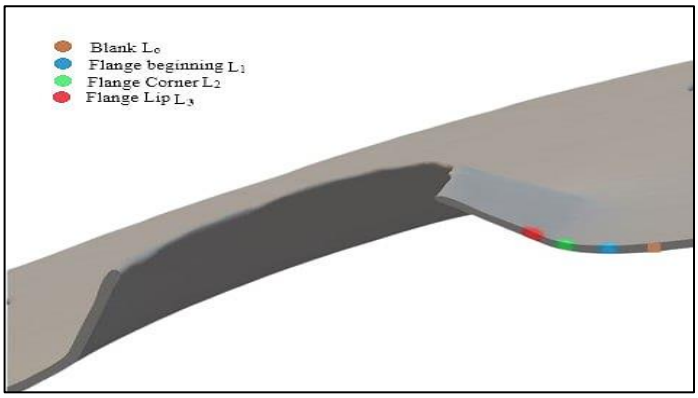

Figure 10: Location of hardness test on flange profile

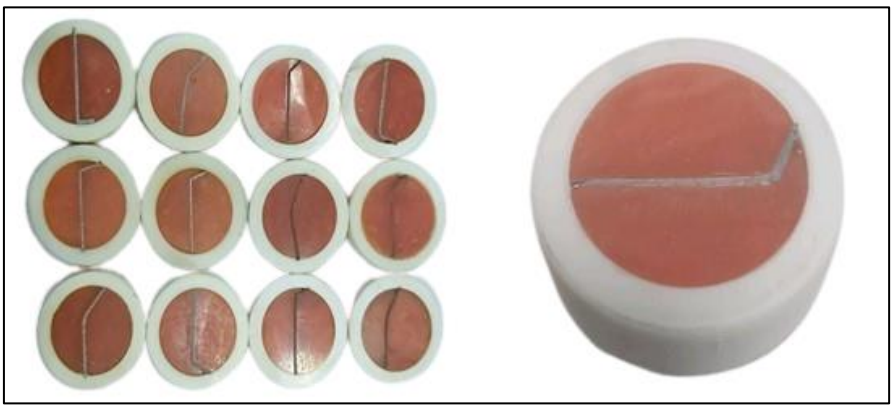

Figure 11: Micro hardness samples preparation and mounting

Figure 12: T-Test model Vickers hardness tester

2.6 Through thickness surface quality test:

In the present experimental work, a thickness surface quality test is conducted to investigate the presence of crack initiation at the fracture initiation location through the specimen thickness based on test dependence on the specimen thickness [22]. As shown in Figure 13, a variable speed grinder-polisher machine is used with several Emery paper of (200,400,600,800,1000,1200,2000) for grinding mounted specimens. As well as for polishing of grinded specimens, an aluminum Oxide of 50 Micron paper was used.

For etching purposes, the steel specimens were immersed in 2 ml nitric acid 100 ml (ethanol/alcohol) for 5 seconds. Then, they were dried by an air dryer. At the same time, for aluminum, the specimens were immersed for 30 seconds in nitric acid, hydrochloric acid, and methanol, each 25 ml and one drop of hydrofluoric acid, drying it by air dryer [23]. Optical microscopy model Opt scopes Classic 40X-2000X Digital With 5.0Mp Md500 CMOS Microscope was used to examine the surface quality of flange specimens, as shown in Figure 14.

Figure 13: Speed grinder-polisher machine

Figure 14: Classic 40X-2000X Digital optical microscopy

3. Results and discussion

In this study, the hole flanging process of steel sheet DC01 and aluminum sheet AA 1050 of two thicknesses, 0.7 mm and 1 mm carried out using a flanging tool with a modified profile and tool holder to impart rolling and spinning motion during the forming process. A series of incremental hole flanging tests are performed using wall angles of (45°, 72°, and 90°) and forming speeds of (170, 350, and 525) rev/min.

3.1 Formability analysis

A series of 36 tests of incremental hole flanging processes was conducted s, such that each test run of the forming process starts with a 20 mm pre-cut hole and ends with a hole diameter that satisfies the maximum forming ratio for each material type and thickness. Figure 15 represents the successful cylindrical flanges formed at the last stage of the incremental hole-flanging process. The results indicated that different forming angles (wall angles) produce different flange profiles, providing different

forming limits and strain distribution along the forming path. Thus, the forming angle should be carefully selected to obtain better flange profile, thickness, strain distribution, and maximum formability ratio.

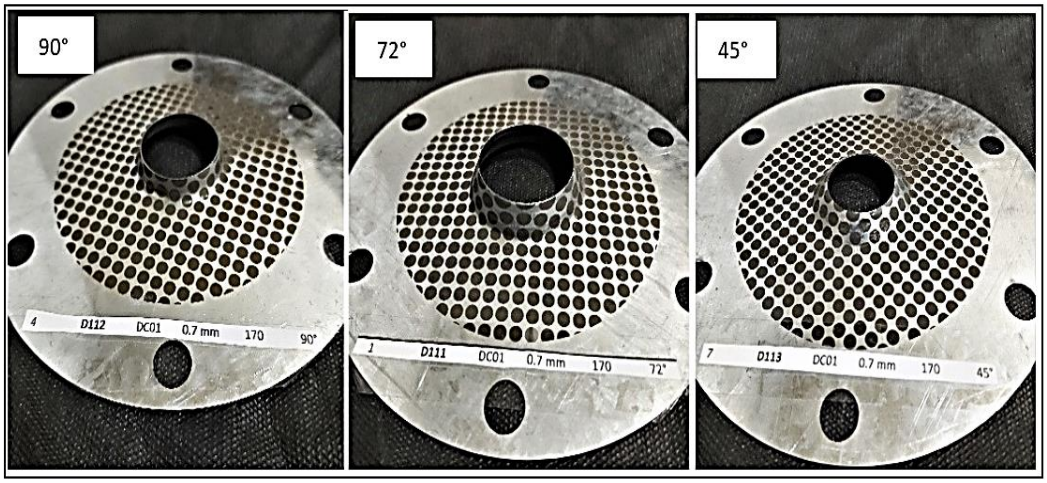

Figure 15: Hole flange profile at different forming angles

The forming limit diagram (FLD) is widely accepted as a conventional approach for characterizing and evaluating forming limits in diverse sheet metal forming processes, where localized necking and fracture occurrences are well-established. To examine the influence of the forming angle on the FLD trend in the incremental hole flanging process, mechanical grid patterns applied to the surfaces of the sheet metal specimens, and the strain measurements carried out along the flange profile [24]. The forming limit curve can be generated using the experimental data using Nakajima's equation as appear in equation 5 [24].

$$FLC = \varepsilon_{major} + \frac{\varepsilon_{major}^2}{\varepsilon_{minor}} \quad (5)$$

Where, FLC is the forming limit curve, and ε_{major} and ε_{minor} are the major and minor strains.

Figures 16(a) and (b) show the forming limit diagram of DC01 steel sheets for the maximum flange height gathered from experimental tests at forming speed of 350 rpm and forming angle of 72° for specimen thickness of 0.7 mm and at forming speed of 170 rpm and forming angle of 72° for specimen thickness of 1 mm respectively. The diagram indicates that the induced strains due to the forming process do not exceed the maximum limit irrespective of the forming speed as compared with the forming limit curve [16], which in turn shows that the proposed tool may enhance the formability of the incremental hole flanging by satisfying maximum lip height without initiation of cracks at the end of the process in comparison with traditional one. As well as the diagram also focuses on the fact that the forming process is carried out initially by uniaxial stress. Then the major strain increases toward the corner of the flange, which indicates the predominantly of the uniaxial forming stress. Consequently, as the forming process goes ahead toward the end of the process, the stress states may be changed or not determined by the thickness of the specimens, as can be seen in the FLD of the DC01 steel sheet of 1 mm thickness in comparison to that of the specimen DC01steel sheet of 0.7 mm thickness.

Furthermore, the formability is significantly affected by the spindle speed and sheet thickness. A successful forming of components without fracture was achieved with the combination of higher spindle speed and sheet thickness. The correlation between increased formability and sheet thickness is linked to the material's mechanical properties.

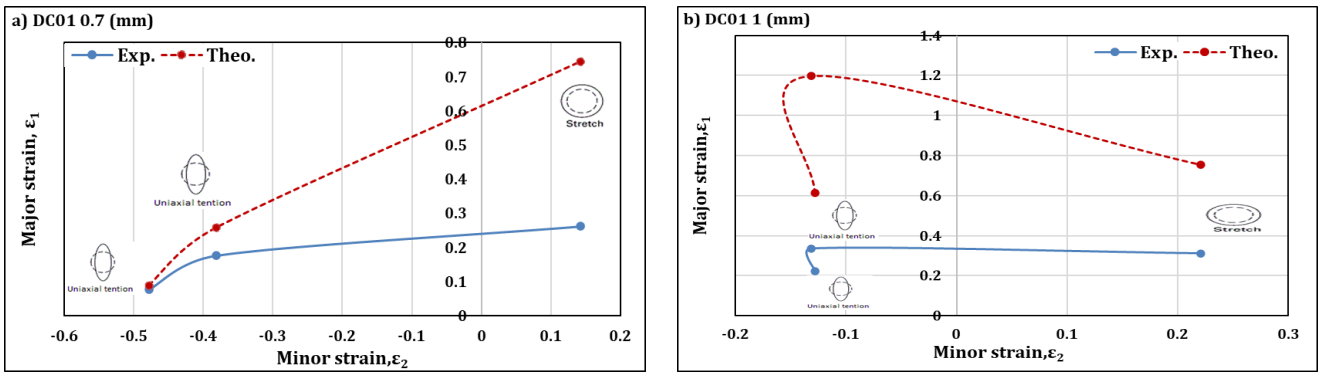

Figure 16: FLD for steel sheets: a) 0.7mm thickness, and b) 1 mm thickness

Figures 17(a) and (b) show the forming limit diagram of AA1050 aluminum sheets for the maximum flange height gathered from experimental tests at forming speed of 350 rpm and forming angle of 45^o for specimen thickness of 0.7 mm and at forming speed of 170 rpm and forming angle of 72^o for specimen thickness of 1 mm respectively. It is worth noting that the FLD curves in terms of minor and major strains revealed that the strains induced due to incremental hole flanging process do not exceed the safe limit irrespective of the forming angle compared with the experimental results of FLD of aluminum sheets [15]. Consequently, this emphasizes that the present tool can successfully achieve the incremental hole flanging process without indicating the possibility of initiating cracks and avoiding the growth of the minor strain towards failure by fracture upon the end of the process. Also, the formation and increase in the minor strain is greatly affected by the material thickness, which in turn impart increases in minor strain without exceeding the forming limit of the material, such that AA1050 sheet of 1 mm compared with 0.7mm. The forming limit diagram (FLD) shows the extremely affected of the rising forming angle, and the critical major and minor strains were generated with higher wall angles. DC04 carbon steel at different wall angles exhibits roughly good results compared to AA1050 aluminum alloy [15].

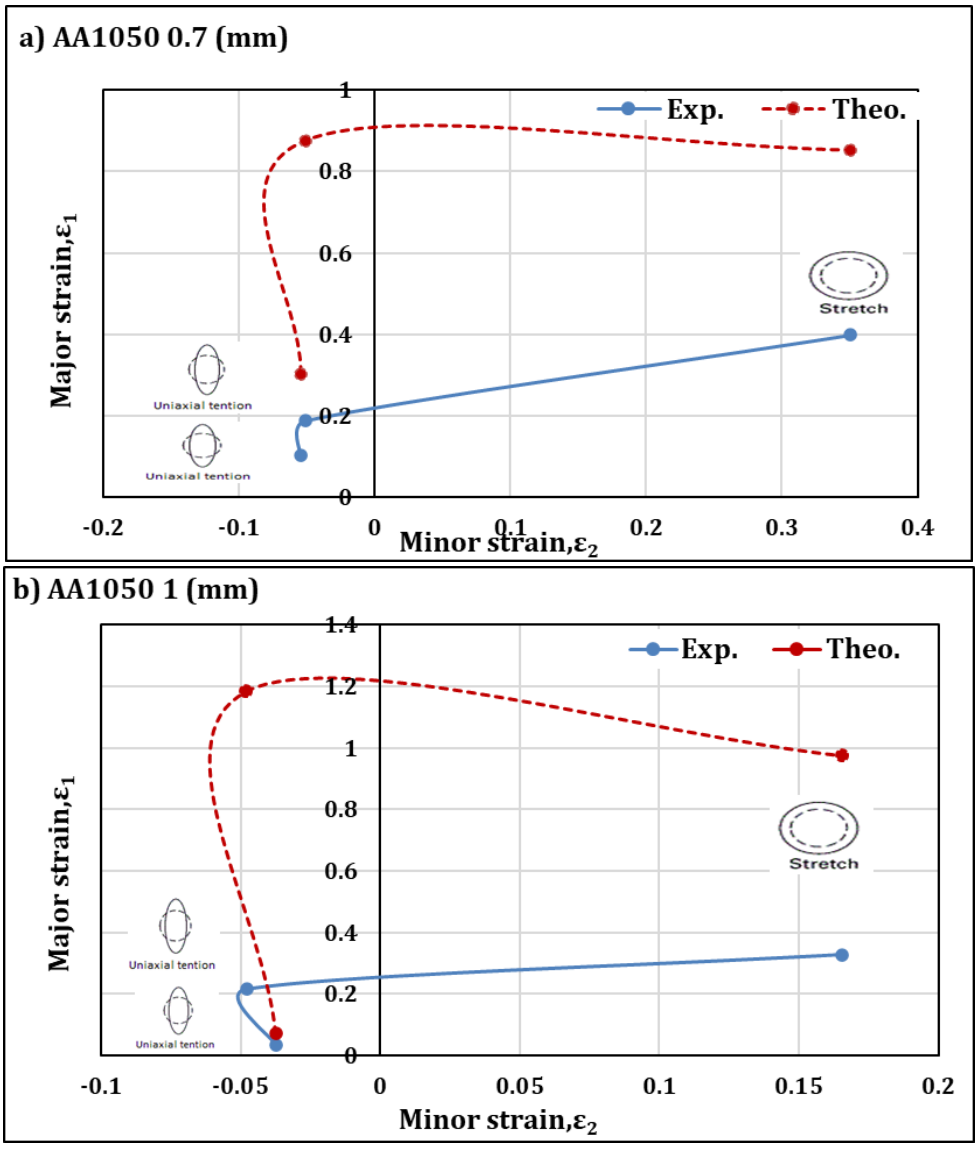

Figure 17: FLD for aluminum sheets: a) 0.7mm thickness, and b) 1 mm thickness

The preceding figures of FLD indicated that the curves exhibit two different deformation modes. Firstly, the positive part of the curve indicates that the deformation of a stretch mode is formed with a biaxial strain condition applied by the forming tool. Secondly, the negative part of the FDL curve shows a deformation shift from a biaxial to a uniaxial pattern [17]. Accordingly, these deformation modes show that the sheet blanks initially deform with a stretching operation at the beginning of the process and subsequently go under deformation consisting of circumferential and longitudinal one with the fact that the transformation of deformation mode is typically controlled by the thickness, type of metal sheet, and the forming speed. Further, the observations of the formability, as depicted in the figures above, demonstrate that the wall flanges in incremental forming can be severed from different deformation zones. These zones include the zone where deformation occurs without any cracks. The severe thinning zone refers to the flange part that undergoes excessive thickness reduction. The crack zone

provides insight into crack initiation, which may be the site of the first crack, and finally, the crack zone, which represents the last zone in the observations of formability [15]. Accordingly, the forming limit diagram of the aluminum sheet of 1 mm shows an intersection between the safe limit and the experimental one, which may indicate an access stretching and strains induced at the tip of the flange wall, as shown in Figure 18. Based on that, the tool produces fracture at the initial stage of the formed components for 1 mm aluminum sheet thickness. Finally, the results indicated that the steel sheet DC01 at different forming angle exhibits roughly good results in comparison with AA1050 aluminum sheet.

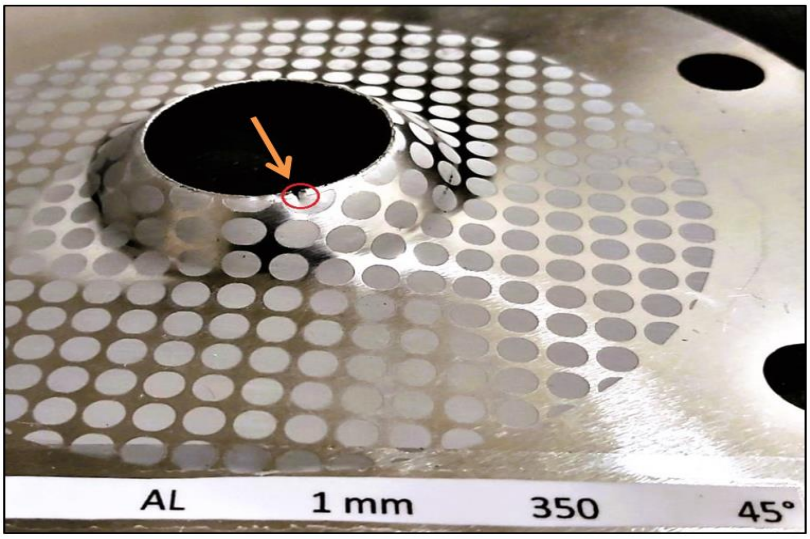

Figure 18: Cracked wall at the tip of the flange

3.2 Hardness analysis

The influence of the forming speed and forming angle on the microhardness of the incremental hole flanging process for steel DC01 and aluminum AA1050 are shown in Figures 19(a) and (b) and Figure 20(a) and (b), respectively. To explain the amount of change in microhardness along the flange profile is compared to the specimen hardness before deformation, the microhardness in these figures is expressed in terms of percentage microhardness, which represents the percentage ratio of the post hardness value at the lip of the flange for each run test to the specimen hardness before deformation. Generally, in all hardness tests, the results show an increase in the post-hardness of the material sheet. The variation in the metal's hardness is entirely controlled by the forming speed and forming angle for each sheet material type and thickness, with observing a transition situation in the post-hardness trend determined by forming speed at 350 rpm, irrespective of the forming angle. Consequently, carefully selecting the forming speed and forming angle enhances the final hardness values for the incremental hole-flanging process. The hardness variation may be attributed to increases thinning of metal in the deformation region when the strain changes from uniaxial mode to the biaxial mode due to the change in forming speed or forming angle, which in turn is responsible for the corresponding decreases in the hardness [18].

Finally, the hardness results indicated a noticeable difference in hardness values of the steel and aluminum sheets due to their differences in mechanical properties, showing maximum and minimum hardness values at different forming angles and forming speeds. The maximum increase in post hardness does not exceed 73% for steel sheets observed at forming angles of 72^{o} for 0.7 mm thickness and a 15 % increase in post hardness at forming angles of 90^{o} for 1 mm sheet thickness, respectively. While, for the aluminum sheet, the maximum increase in post hardness does not exceed 6% and 8% observed at forming angles of 90^{o} for both 0.7 and 1 mm sheet thicknesses, respectively.

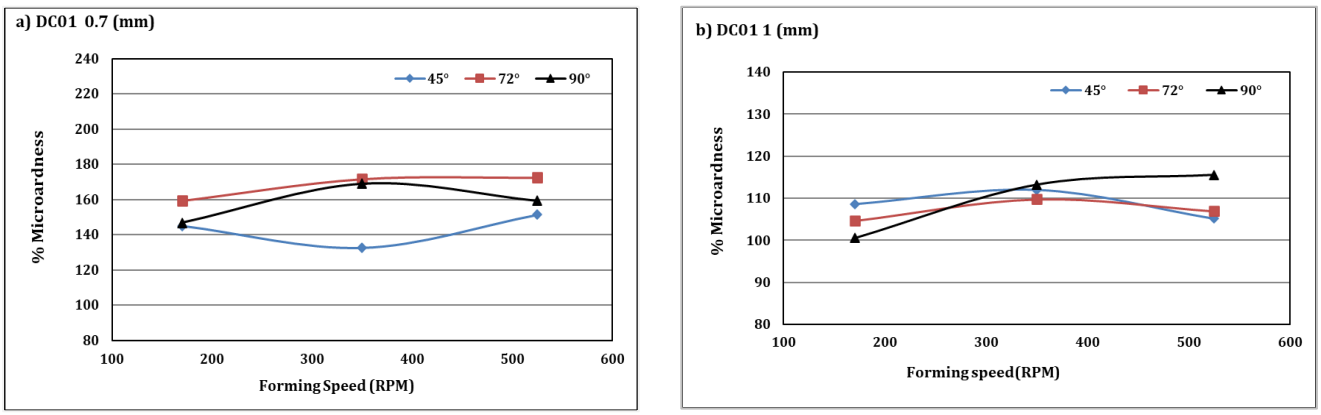

Figure 19: Variation of percentage hardness with forming speed for steel sheet:a) 0.7 mm thickness, and b)1mm thickness

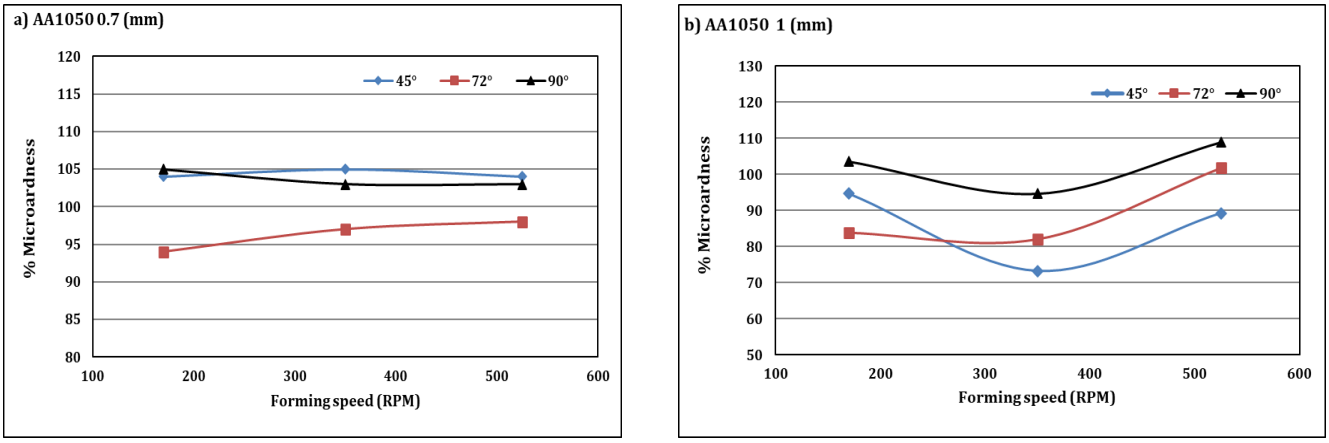

Figure 20: Variation of percentage hardness with forming speed for aluminum sheet: a) 0.7 mm thickness, andb)1mm thickness

The hardness distribution over the flange profile is shown in Figures 21(a) and (b), and 22(a) and (b) for steel and aluminum sheets of 0.7 mm and 1 mm thicknesses at forming angles of 72^{o} and forming speed of 170 rpm for steel sheets, while at forming angle of 45^{o} and forming speed of 350 rpm for aluminum sheets respectively. The results revealed an increase in the hardness of sheet metals over the flange profile with respect to the distance from the specimen root (un-deformed base), with different trends reflecting the differences in material types and thicknesses [18]. Also the lip height shows different heights corresponding to material capacity while experiencing as much as possible amount of deformation without a tendency toward crack initiation with increases in material hardness at the end of the hole flanging process. Also, the maximum hardness induced does not exceed the allowable values because all the test runs do not show an obvious crack or earning over the final flange profile.

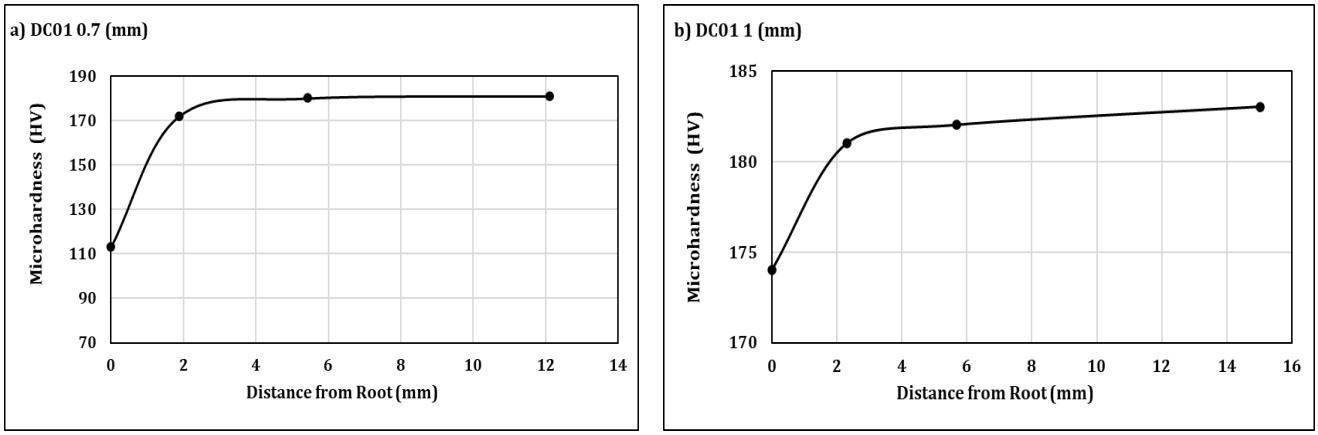

Figure 21: Hardness distribution with distance from flange root for steel sheet: a) 0.7 mm thickness, and b)1mm thickness

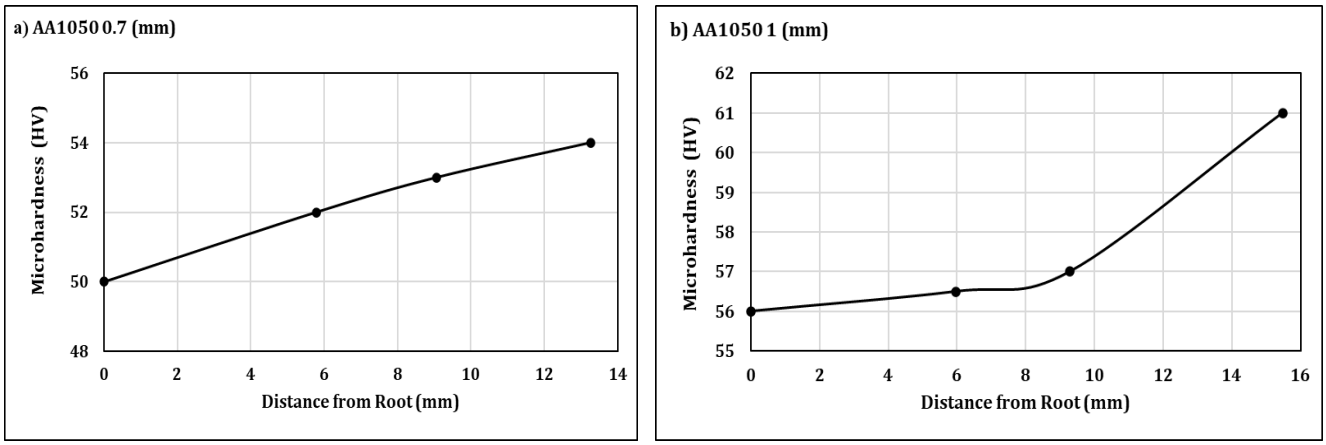

Figure 22: Hardness distribution with distance from flange root for aluminum sheet: a) 0.7 mm thickness, and b)1mm thickness

3.3 Thickness analysis

The results of examining the thickness variation with forming speed and forming angle are depicted in Figures 23(a) and (b), and 24(a) and (b) for steel and aluminum sheets, respectively, at the lip of the flange. All the experimental results deduced that the thickness variation with a forming speed experienced different percentage ratios. However, the variation is still within the expected range of thickness reduction. There is no evidence of crack initiation, especially for the maximum thickness variation of 92% at 170 rpm and 0.7 mm steel sheet. This revealed that the proposed tool profile and fixture enhanced formability. Also, the tool starts deformation with bending at the initial stages, avoiding the overstretching along the deformation path, and the forming speed and forming angle can greatly control the thickness variation by controlling the deformation modes from uniaxial modes to biaxial modes. Consequently, it can be seen that there is a forming speed at which the variation trend can be changed and altered critically. Thus, the forming speed and form selection should be carried out carefully to obtain a good formability limit in the incremental hole-flanging process. This may be attributed to the increase in the forming speed, which reduces the friction and increases temperature, reducing the forming force and stretching stresses, promoting a lower thickness variation in the deformation zone [19].

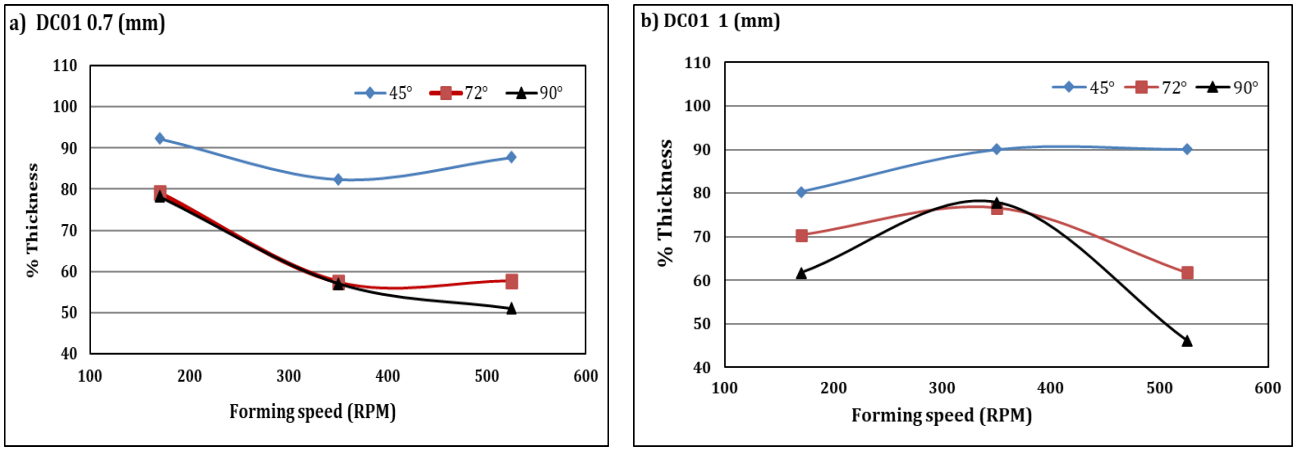

Figure 23: Variation of percentage thickness with forming speed for steel sheet: a) 0.7 mm thickness, and b)1mm thickness

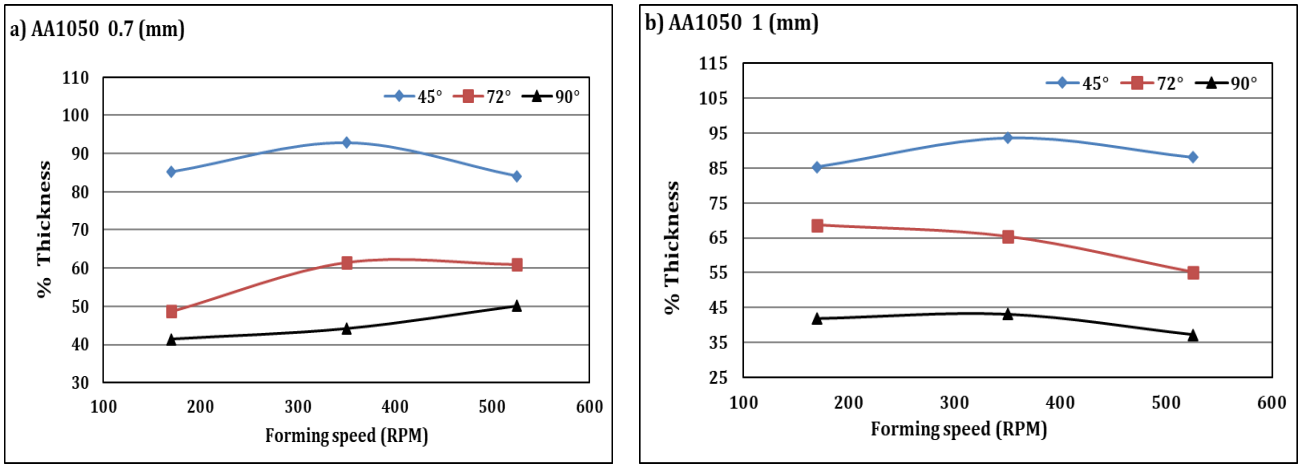

Figure 24: Variation of percentage thickness with forming speed for aluminum sheet: a) 0.7 mm thickness, and b)1mm thickness

The thickness distribution along the flange profile is explained in Figures 25(a) and (b) and 26(a) and (b), respectively, for steel and aluminum sheets at forming angles of 72^o and forming speed of 170 rpm for steel sheets, while forming an angle of 45^o and forming speed of 350 rpm for aluminum sheets used respectively. The results indicated a smooth thickness distribution along the flange profile with no obvious large thinning occurring due to changes in deformation modes, and most of the change in thickness occurs at the middle distance [14], revealing that the proposed tool profile and holding arrangement deduce good formability and enhances the incremental hole flanging process over a low range of forming speeds. Also, the results show that the maximum reduction in thickness of steel sheet does not exceed 35% for 0.7 mm thickness and 40% for 1 mm thickness at a speed of 170 rpm and forming an angle of 72^o. For aluminum sheets, the results indicate a maximum reduction in thickness does not exceed 39% for 0.7 mm sheet thickness and 51% for 1 mm sheet thickness at a forming speed of 350 and forming angle of 45^o. The differences in thickness reduction ratios may be related to the differences in material properties of steel and aluminum sheets. Finally, the maximum thickness reduction leads to heights lip height as depicted by Figures 25(b) and 26(b) for larger sheet thicknesses of (1mm) in compared to the lowest lip height corresponding to the minimum thickness reduction of the smaller sheet thickness of (0.7 mm), as indicated by Figures 25(a) and 26(a).

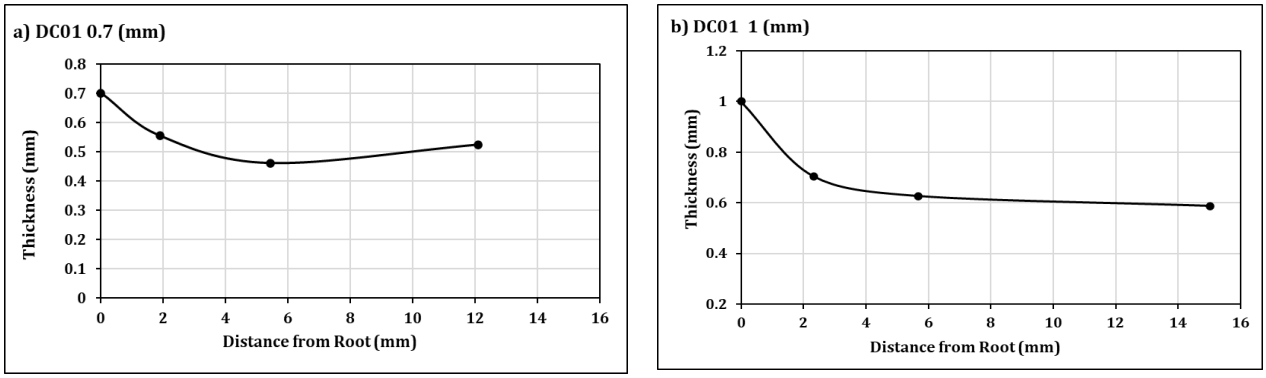

Figure 25: Thickness distribution along flange profile for steel sheet: a) 0.7 mm thickness, and 1 mm thickness

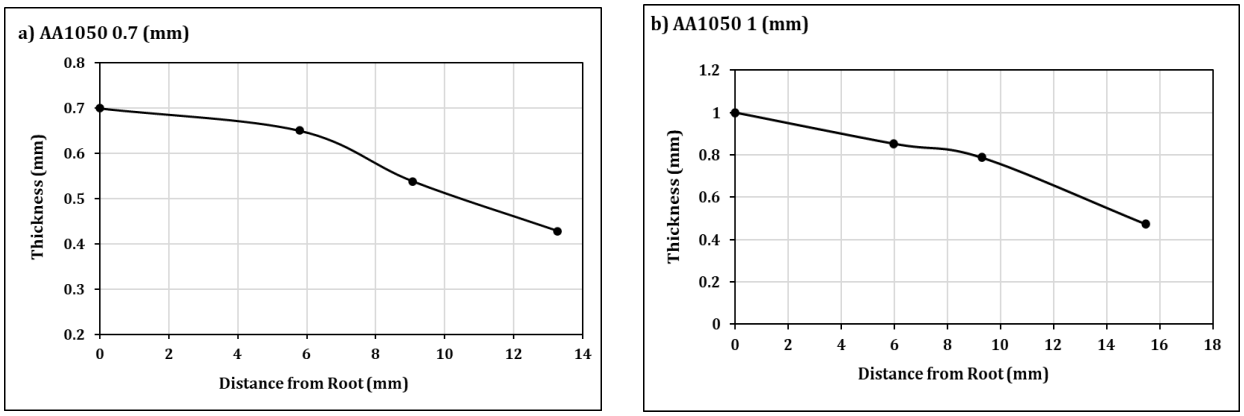

Figure 26: Thickness distribution along flange profile for aluminum sheets: a) 0.7 mm thickness, and 1 mm thickness

3.4 Surface quality

A series of through-thickness surface quality (topography) tests were carried including the specimens with maximum height flange only corresponding to each forming angles of (45^o and 72^o) and for both types of sheet metals and thickness at L_1, L_2, and L_3 locations are shown in Figures 27 and 28 respectively. These tests are conducted through the cross-section of the specimen thickness at the tip of the flange height and the flange corner. In contrast, these locations are severed from maximum deformation during the hole-flanging process, and the large possibility of cracks or section thinning may be presented at these locations. In general, the results indicated different surface topographies corresponding to different forming speeds, forming angles, sheet materials, and sheet thicknesses, which may be attributed to the differences in the mechanical properties of the metal sheets [14]. Further, the test results show a good surface quality and free of localized cracks and or excessive thinning of the deformed sheet during the deformation process carried out by incremental hole flanging technique.

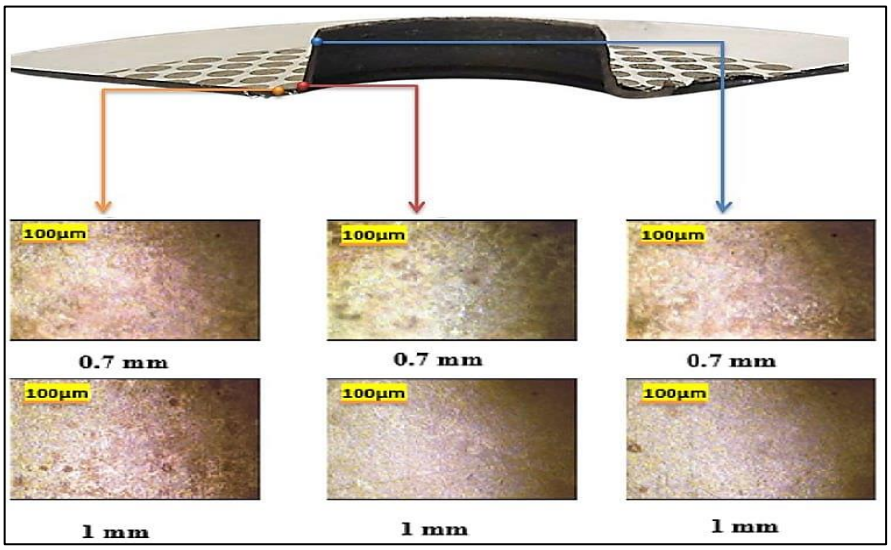

Figure 27: Through thickness surface topography of steel sheet of 0.7 mm and 1 mm at forming speed of 170 rpm

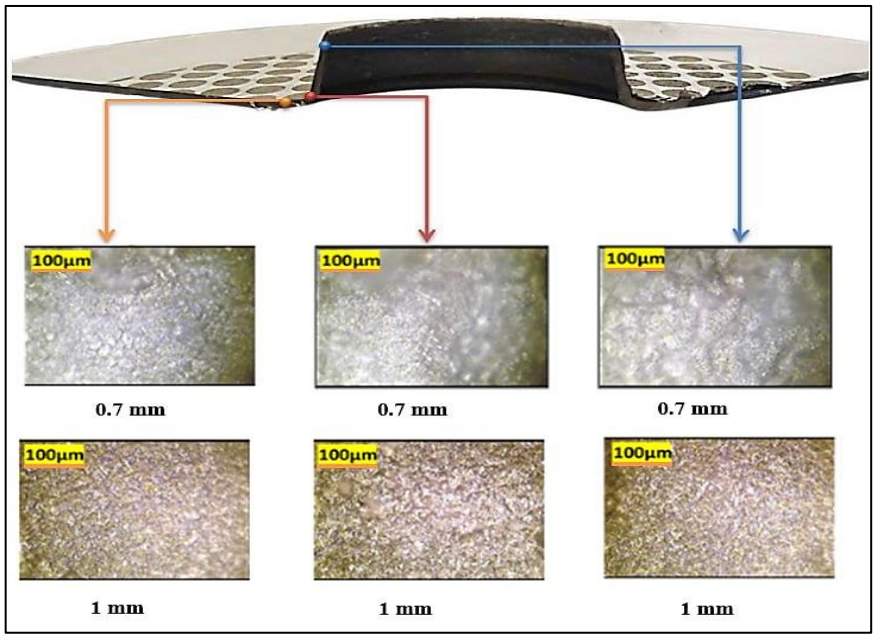

Figure 28: Through thickness surface topography of aluminum sheet of 0.7 mm and 1 mm at forming speed of 170 rpm

4. Conclusion

The present experimental work provided comprehensive insights into the influence of forming speeds and forming angles on the microhardness and thickness variations and the microhardness and thickness distribution along flange profiles for various sheet materials and thicknesses based on the proposed tool geometry and tool mounting and fixture. These findings contribute valuable information for optimizing incremental hole-flanging process parameters. The main conclusions of the present work may be summarized as follows:

1) The formability of sheet metals is significantly affected by forming speed and sheet thickness. The relationship is directly proportional, indicating that formability increases with increasing forming speed and sheet metal thickness. For example, in sample DC01, with a thickness of 0.7 mm and forming speed of 350 rpm, with a wall angle of 72°, the major strain was 0.262. Conversely, in sample DC01, with a thickness of 1mm and forming speed of 170 rpm, with a wall angle of 72°, the major strain was 0.312.
2) The Forming Limit Diagram (FLD) results indicate that the formability of sheet metals is significantly affected by forming speed and sheet thickness. The relationship is directly proportional, meaning that formability increases with increasing forming speed and sheet metal thickness. For instance, in sample AA1050, with a thickness of 0.7mm, at a forming speed of 350 rpm and a wall angle of 45°, the major strain was 0.359. In contrast, in sample AA1050, with a thickness of 1mm, at a forming speed of 170 rpm and a wall angle of 45°, the major strain was 0.398.
3) Regarding hardness, the percentage with a wall angle of 72° with respect to forming speeds of 170, 350, and 525 rpm significantly affected the increase in micro-hardness percentage for DC01 0.7 mm. The maximum micro-hardness percentages were 159%, 169%, and 172%, respectively. Similarly, with a wall angle of 45°, the micro-hardness percentage significantly increased for AA1050 0.7 mm, with maximum percentages of 104%, 105%, and 104% at forming speeds of 170, 350, and 525 rpm, respectively.
4) Micro-hardness distribution over the flange profile increased from the base (113 HV) to 181 HV at the end for DC01 0.7mm, at a forming speed of 170 rpm and a wall angle 72°. This represents a 60% enhancement in micro-hardness over the entire flange profile. Similarly, for AA1050 1 mm, micro-hardness distribution increased from 56 HV to 61 HV at the end of the flange profile at a forming speed of 170 rpm and a wall angle of 45°.
5) Percentage thickness reduction during the hole flanging process indicated that the better wall angle for DC01 0.7mm was 45°, with overall flange profile thickness remaining at 92%, 82%, and 87% of the initial thickness for forming speeds of 170, 350, and 525 rpm, respectively. Likewise, for AA1050 1 mm, the better wall angle was 45°, with overall flange profile thickness remaining at 85%, 93%, and 88% of the initial thickness for the same forming speeds.
6) Surface quality results revealed that for DC01 sheet metal, significantly affected parameters were 350, 170 rpm, and a wall angle of 72°, respectively. Additionally, observations showed that surface quality was less affected with lower forming speeds. Similarly, for AA1050 sheet metal, significantly affected parameters were 350, 170 rpm, and a wall angle of 45°. Again, lower forming speeds had a lesser impact on surface quality.
7) The formability results indicated that the deformation strains were within the safety limit, and the DC01 steel sheet exhibited better formability than AA1050 aluminum sheets.
8) The uniform and smooth thickness distribution along the flange profile indicated an enhancement in formability ratio with no obvious large thinning occurring due to changes in deformation modes.

5. Future research

The scope of the current research work was dedicated to investigating the effect of tool profiles and fixtures with specific geometry. This knowledge can be further extended to include more complicated profiles based on verified finite elements models using ANSYS/workbench/Dynamic explicit software. Also, the hot forming process can be studied numerically.

Author contributions

Conceptualization, H. Lafta, and A. Shahab; methodology, H. Ali; software, H. Ali; validation, H. Lafta, and A. Shahab; formal analysis, H. Lafta.; investigation, H. Ali.; resources, H. Ali.; data curation, H. Ali.; writing—original draft preparation, H. Ali.; writing—review and editing, H. Lafta.; visualization, H. Ali.; supervision, H. Lafta, and A. Shahab; project administration, H. Lafta. All authors have read and agreed to the published version of the manuscript.

Funding

This research received no specific grant from any funding agency in the public, commercial, or not-for-profit sectors.

Data availability statement

The data that support the findings of this study are available on request from the corresponding author.

Conflicts of interest

The authors declare that there is no conflict of interest.

References

[1] M. Borrego, D. Morales-Palma, J. A. López-Fernández, A. J. Martínez-Donaire, G. Centeno, C. Vallellano, Hole-flanging of AA7075-O sheets: conventional process versus SPIF, Procedia Manuf., 50 (2020) 236-240. https://doi.org/10.1016/j.promfg.2020.08.044

[2] Saidi, B. Experimental and numerical study of the hot incremental forming process of titanium sheets, PhD. Thesis, University of Technology of Troyes; National School of Engineers of Tunis, Tunisia, 2018. https://theses.hal.science/tel-03211429

[3] S. Gatea, H. Ou, G. McCartney, Review on the influence of process parameters in incremental sheet forming, Int. J. Adv. Manuf. Technol., 87 (2016) 479-499. https://doi.org/10.1007/s00170-016-8426-6

[4] Y. Fang, B. Lu, J. Chen, D. Xu, H. Ou, Analytical and experimental investigations on deformation mechanism and fracture behavior in single point incremental forming, J. Mater. Process. Technol., 214 (2014) 1503-1515. https://doi.org/10.1016/j.jmatprotec.2014.02.019

[5] S. Kumar, M. Ahmed, S. K. Panthi, Effect of punch profile on deformation behaviour of AA5052 sheet in stretch flanging process, Arch. Civ. Mech. Eng., 20 (2020) 1-17. https://doi.org/10.1007/s43452-020-00016-2

[6] M. Durante, A. Formisano, A. Langella, F. M. Minutolo, The influence of tool rotation on an incremental forming process, J. Mater. Process. Technol., 209 (2009) 4621-4626. https://doi.org/10.1016/j.jmatprotec.2008.11.028

[7] L. I. Besong, J. Buhl, M. Bambach, Increasing formability in hole-flanging through the use of punch rotation based on temperature and strain rate dependent forming limit curves, Int. J. Mater. Form., 15 (2022) 37. https://doi.org/10.1007/s12289-022-01684-6

[8] M. Laugwitz, H. Voswinckel, G. Hirt, M. Bambach, Development of tooling concepts to increase geometrical accuracy in high speed incremental hole flanging, Int. J. Mater. Form., 11 (2018) 471-477. https://doi.org/10.1007/s12289-017-1356-5

[9] M. Silva, P. Teixeira, A. Reis, P. Martins, On the formability of hole-flanging by incremental sheet forming, J. Mater. Des. Appl., 227 (2013) 91–99. https://doi.org/10.1177/1464420712474210

[10] P. K. Gandla, S. Pandre, K. Suresh, N. Kotkunde, A critical analysis of formability and quality parameters for forming a dome shape using multi-stage strategies in incremental forming process, J. Mater. Res. Technol., 19 (2022) 1037-1048. https://doi.org/10.1016/j.jmrt.2022.05.064

[11] L. Montanari, V. Cristino, M. B. Silva, P. A. Martins, A new approach for deformation history of material elements in hole-flanging produced by single point incremental forming, Int. J. Adv. Manuf. Tech., 69 (2013) 1175-1183. https://doi.org/10.1007/s00170-013-5117-4

[12] V. Cristino, L. Montanari, M. Silva, A. Atkins, P. Martins, Fracture in hole-flanging produced by single point incremental forming, Int. J. Mech. Scien., 83 (2014) 146-154. https://doi.org/10.1016/j.ijmecsci.2014.04.001

[13] M. Laugwitz, H. Voswinckel, G. Hirt, M. Bambach, Development of tooling concepts to increase geometrical accuracy in high speed incremental hole flanging, Int. J. Mater. Form., 11 (2018) 471-477. https://doi.org/10.1007/s12289-017-1356-5

[14] M. T. Mezher, S. M. Khazaal, N. S. Namer, R. A. Shakir, A comparative analysis study of hole flanging by incremental sheet forming process of AA1060 and DC01 sheet metals, J. Eng. Sci. Technol., 16 (2021) 4383-4403. https://jmerd.net/Paper/Vol.44,No.1(2021)/337-345.pdf

[15] M. T. Mezher, O. S. Barrak, S. A. Nama, R. A. Shakir, Predication of Forming Limit Diagram and Spring-back during SPIF process of AA1050 and DC04 Sheet Metals, J. Mech. Eng. Res. Dev., 44 (2021) 337-345.

[16] R. Vasile, S.-G. Racz, O. Bologa, Experimental and numerical investigations of the steel sheets formability with hydroforming, MATEC Web of Conferences, 94, 2017, 02016. https://doi.org/10.1051/matecconf/20179402016

[17] G. Centeno, M. Silva, V. Cristino, C. Vallellano, P. Martins, Hole-flanging by incremental sheet forming, Int. J. Mach. Tools Manuf., 59 (2012) 46-54. https://doi.org/10.1016/j.ijmachtools.2012.03.007

[18] M. T. Mezher, R. A. Shakir, Modelling and evaluation of the post-hardness and forming limit diagram in the single point incremental hole flanging (SPIHF) process using ANN, FEM and experimental, Results Eng., 20 (2023) 101613. https://doi.org/10.1016/j.rineng.2023.101613

[19] M. B. Puche, Analysis of single stage SPIF process applied to the hole flanging operation, PhD Thesis, Universidad de Sevilla, 2018.

[20] R. Baptiste, D. L. Clark, P. Matin, Designing a Strain Measurement System based on Circle Grid Analysis for Sheet Metal Forming Applications, ASEE Annual Conference & Exposition, , Columbus, Ohio, 2017. https://doi.org/10.18260/1-2--28125

[21] ASTM E92-17: Standard Test Methods for Vickers Hardness and Knoop Hardness of Metallic, ASTM Int., 82 (2018) 1-27. https://doi.org/10.1520/E0092-17.2

[22] I. Peshekhodov, M. Dykiert, M. Vucetic, B.-A. Behrens, Evaluation of common tests for fracture characterisation of advanced high-strength sheet steels with the help of the FEA, in IOP Conference Series: Materials Science and Engineering, 159, 2016, 012014. https://doi.org/10.1088/1757-899X/159/1/012014

[23] M. Mohammadtaheri, A new metallographic technique for revealing grain boundaries in aluminum alloys, Metallogr. Microstruct. Anal., 1 (2012) 224-226. https://doi.org/10.4172/jma.1000110

[24] ASTM E2218-15, Standard test method for determining forming limit curves, ASTM Book of Standards, (2015) 1-15. https://doi.org/10.1520/E2218-15

[25] Yu, L., Liu, J., Ge, R., Wei, X., Peng, Z., Chen, M., & Liu, J.. Fracture characteristics and mechanisms of DP780 dual-phase steel under different strain states. Forging Technology, 47, (2022) 48-55. https://doi.org/10.13330/j.issn.1000-3940.2022.08.037